Available online at www.sciencedirect.com
ScienceDirect
Trans. Nonferrous Met. Soc. China 32(2022) 273−284
Transactions of Nonferrous Metals Society of China
www.tnmsc.cn

Deep metallogenic mechanism in southeastern China based on receiver function data

Jian-xin LIU[1,2,3], Syed muzyan SHAHZAD[1,2,3], Ya SUN[1,2,3], Asim SHAHZAD[1], Chuan LI[4], Meryem FANIDI[1,2], Ishfaque MUHAMMAD[1]

1. School of Geosciences and Info-physic, Central South University, Changsha 410083, China;
2. Key Laboratory of Metallogenic Prediction of Nonferrous Metals and Geological Environment Monitoring, Ministry of Education, Central South University, Changsha 410083, China;
3. Hunan Provincial Key Laboratory of Nonferrous Resources and Geological Hazard Detection, Central South University, Changsha 410083, China;
4. College of Earth Sciences, Guilin University of Technology, Guilin 541006, China

Received 9 February 2021; accepted 28 December 2021

Abstract: Crustal deformation and deep metallogenic mechanisms in southeastern (SE) China are still debated. In this study, we applied the receiver function method to measure crustal thickness and Poisson's ratio for crustal rock using teleseismic data recorded at 207 seismic stations from China Earthquake Administration Network. The results showed that crustal thickness varied from ~27 km in the eastern part to ~43 km in the western part of the study area, with an average crustal thickness of 31 km. The crust is thick in the west and thin in the east. The observed Poisson's ratio for crustal rock was relatively high in the southern Cathaysia Block (CB), with an average of 0.295, while in the Qinling—Dabie terrane, it was relatively low, with an average of 0.257. In the middle of the Yangtze craton and central east of the CB, Poisson's ratio for crustal rock varied from 0.257 to 0.286. By comparing Poisson's ratio of the intrusive deposits with that of igneous rocks in volcanic complexes, we deduced that the metallic mineral system might be associated with orogenic and hydrothermal deposits. These results indicated that multistage magma and mineralization in the study area might be attributed to the tectonic-magma-thermal event. The high Poisson's ratio for crustal rock in the southeastern margin of the CB and northeastern Upper Yangtze Craton might be related to Mesozoic lower crustal mafic partial melt, which provides an important environment for various magmatic intrusions and metallogenies.
Key words: deep metallogenic mechanism; Poisson's ratio; southeastern China; crustal thickness

1 Introduction

There are many important deposits of nonferrous minerals in southeastern (SE) China [1]. SE China was subjected to several phases of the tectonic magmatic processes from the Neoproterozoic to the Cenozoic period [2−6]. The Yanshanian magmatic event was the main reason for triggering regional diagenesis and metallogenesis in this region. The multistage evolution of magma can be categorized by crustal rupture, crustal thinning, intrusion, stretching, shearing, and fluid movement [3]. Yanshanian (Mesozoic−Cenozoic) rifting, magmatism, and basin development played an essential role in establishing the mineral systems in SE China [4−7]. Geological data showed that A-type plutonic rocks in the Cretaceous may derive from a geothermal gradient >40 °C/km [3,5]. These results indicated that the subduction of Paleo-Pacific plate has gone further beneath SE China [5]. Due to Paleo-Pacific

Corresponding author: Ya SUN, E-mail: sunya_seis@csu.edu.cn
DOI: 10.1016/S1003-6326(22)65793-5

subduction and collision between the North China Craton (NCC) and South China Block (SCB), large rifting, wrench faulting, mantle plume activity and magmatic event had occurred between 250 and 155 Ma [6,7]. Meanwhile, igneous activity and mineralization appeared in SE China during the Mesozoic [8,9]. Many types of geophysical measurements (e.g., GPS velocity, magnetotelluric, and seismic tomography) provided constraints on the crustal and upper mantle structure and deformation beneath this region. However, the mechanisms of deformation and the tectonic processes of SE China are still debated.

Seismic methods are generally used to detect mineral resources and explore the deep mineralization mechanism. CHEN et al [10] applied seismic reflection to explore gold deposits. LIU et al [11] detected thrust-controlled mineral deposits by 2D seismic reflection. LUO et al [12] applied seismic tomography in East China and studied mineral deposits in the Middle-Lower Yangtze River Metallogenic Belt (MLYMB). Geodynamic setting, tectono-magmatic activity, lithospheric-structure, and plate subduction might control deep metallogenic mechanism at different stages [13−17]. Seismic receiver function methods can be used to calculate Moho depth and Poisson's ratio. They can provide a relationship between crustal thickness, composition, and background of mineralization mechanism.

In this study, we applied the receiver function technique to measure the crustal thickness and Poisson's ratio for crustal rock. Later on, we used Poisson's ratio to simplify the Poisson's ratio for crustal rock. Combined with geological data and previous geophysical results, we discussed the relationship between the mineralization and Poisson's ratio. These results can provide new insight for exploring metallic mineral deposit resources and deep metallogenic mechanism in SE China.

2 Geological background and tectonic framework

Eastern China was separated into two major tectonic units, the NCC and SCB. The SCB was known as one of the largest cratons in eastern Asia [17−19]. The SCB has been influenced by a long, complex history of subduction of oceanic lithosphere along its extensive eastern and southeastern margins. The west was affected by the collision of the Burma microplate and formed a large-scale complex tectonic evolution [19]. Due to the northeastward extrusion in the west, eastward subduction of the Burma microplate, the extrusion of the uplift Tibetan Plateau and southeastward stretching in the southeast (Fig. 1(a)), large-scale crustal and upper mantle deformation and a diverse range of geological structures have been produced in SE China [20]. Since northwestern extensional

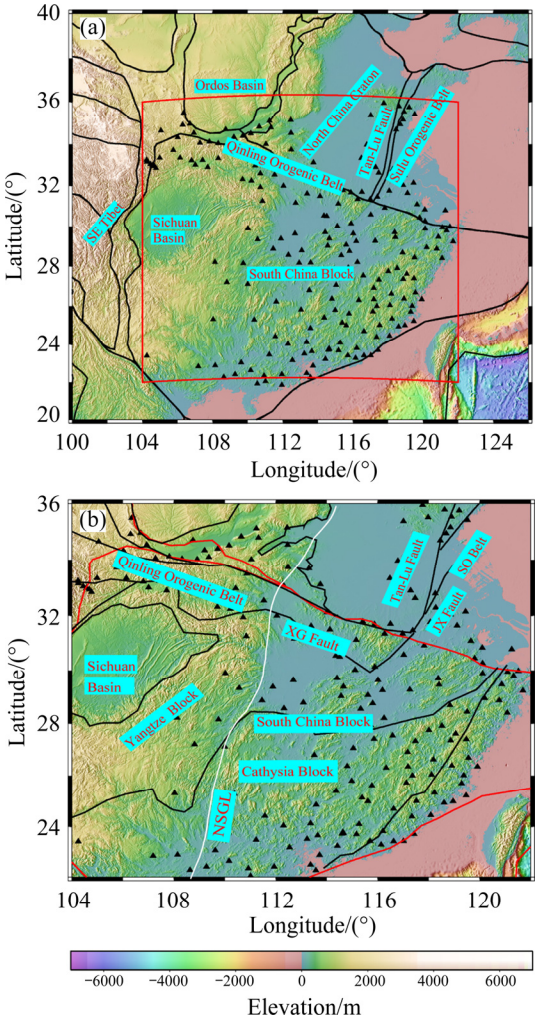

Fig. 1 Topography maps with seismic stations black solid triangles in SE China: (a) Red rectangular portion representing study area and black lines representing mainly faults; (b) Black and red lines representing fault lines and block boundaries respectively (XG: Xiangfan—Guangji Fault; JX: Jiashan—Xiangshui Fault; SO: Sulu Orogen; UYB: Upper Yangtze Block; MYB: Middle Yangtze Block; LYB: Lower Yangtze Block) white line representing North−South trending Gravity Lineament (NSGL)

forces were driven by Philippine plate and Pacific plate subduction, Neoproterozoic−Paleozoic collision also occurred between the Cathaysia Block (CB) and the Yangtze Block (YB) around the Jiangnan Belt (Fig. 1(b)) [20,21].

Since the rolling back of Paleo-Pacific slab relative to the eastern NCC, the Middle-Lower Yangtze Craton has lost its roots. In addition, delamination, subduction to thermochemical erosion and destructive mechanism also appeared during crustal and mantle deformations [22,23]. The Qinling Orogenic Belt (QOB) developed from the early Paleozoic−Mesozoic collision of the NCC and SCB, which can be considered as one of the major suture zones in central China [17]. Qinling—Dabie — Sulu Orogenic Belts or central China Orogenic Belts are the east-west trending interfaces that link the Xiangfan—Guangji and the Xinyang—Shucheng suture zones [23].

3 Data

In this study, we first obtained data from China Earthquake Administration (CEA) Network, in which each station contains three-components broadband seismograph. We then selected 207 seismic stations located between 104° and 122° E, and 22° and 37° N (Fig. 1(b)), recorded between January 2007 and December 2015. A total of 931 teleseismic earthquakes with a magnitude greater than 5.0 and an epicentral distance ranging from 30° to 90° were chosen. Earthquakes provided relatively good coverage for both distance and azimuth (Fig. 2). The basic analysis was carried out in SAC (Seismic Analytic Code), such as filtering, phase picking, rotation, and cutting of the seismogram [23−25]. The heat flow data were collected from the website (https://data.mendeley.com/datasets/f88sxj5jm8/1). As for the Moho temperature data, we utilized the database from previous literature [26,27].

4 Receiver functions

The seismic receiver function method has been widely used to understand continental lithospheric crust and upper mantle structure. This method was usually based on a series of P-to-S converted waves (Ps) at Moho depth [24,25]. Firstly, to generate the

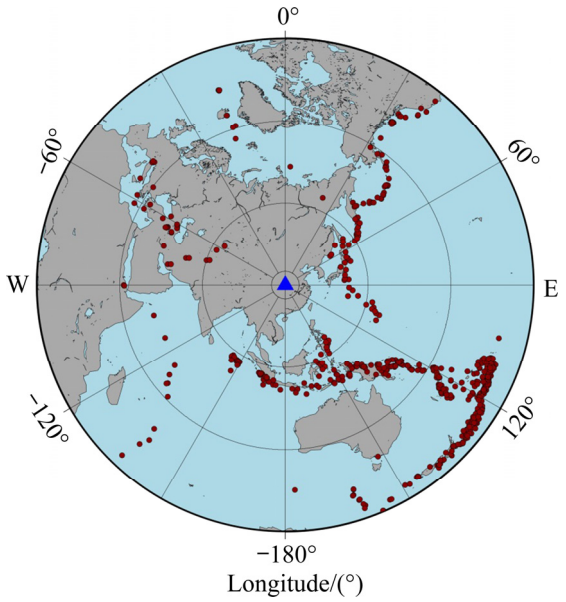

Fig. 2 Event map with 931 teleseismic event locations (dark red solid circles, and most earthquakes located along Java Sumatra trench and Pacific Ocean)

receiver function, we rotated two seismic horizontal components (E, N) to the radial and transverse components based on coordinate system to isolate the converted Ps wave from the direct P wave [25,28]. The receiver functions were then computed from the data projected into this coordinate system (later on referred as to P- and SV-component) [29]. We employed the "water-level" deconvolution in the frequency domain to generate receiver functions [29,30]:

$$RF(\omega)=\frac{V(\omega)\times P^{*}(\omega)}{\max\left\{\left|P(\omega)\right|^{2},k\times\left|P_{\max}(\omega)\right|^{2}\right\}}\exp[\omega/(2a)]^{2} \quad (1)$$

where k and a are two constants that define the "water level" and the corner frequency of the Gaussian low pass filter. k is set to 0.01, and a is 1.5, which is equivalent to a corner frequency of ~0.5 Hz. $P(\omega)$ and $V(\omega)$ are the spectra of the P and SV components, respectively. $P^{*}(\omega)$ is the complex conjugate of $P(\omega)$. ω is the angular frequency. To minimize high-frequency noise, a Gaussian low pass filter was added to the radial receiver function. Data were filtered to produce receiver functions during the deconvolution process. We performed strict data quality, checked all receiver functions visually, and removed those with a low signal-to-noise ratio (SNR).

4.1 *H*–*κ* analysis

We used SV receiver functions in *H*–*κ* stacking domain to measure Moho depth (*H*) and average V_p/V_s ratio (*κ*) for crust at all stations using Eq. (2), where V_p and V_s represent the velocity of P wave and S wave, respectively. The relative arrival time of the converted phase at Moho, Ps, with respect to the direct arrival by ray tracing the two multiple converted phases (1P2s and 2P1s) were first computed using a modified "1D iasp91" model [24,28]. NIU et al [25] introduced a large trade-off between *H* and *κ*, and he used a coherence index of the three phases, *c*(*κ*), to reduce the *H*–*κ* trade-off:

$$S(H,\kappa)=\frac{c(\kappa)}{N}\sum_{i=1}^{N}\{w_1 r_i(t_1)+w_2 r_i(t_2)+w_3 r_i(t_3)\} \quad (2)$$

where *N* is the number of receiver functions at a given station, and $r_i(t)$ represents the amplitude of the *i*th receiver function at the primary P-to-S converted phase Ps(t_1), and the two crustal multiples, 2P1s(t_2) and 1P2s(t_3) (Fig. 3). The weights of the three phases w_1, w_2, and w_3 are equal to 0.5, 0.25, and 0.25, respectively. SV receiver functions and *H*–*κ* stacking results at station ZJ.CHA are shown in Fig. 3 and Fig. 4, respectively.

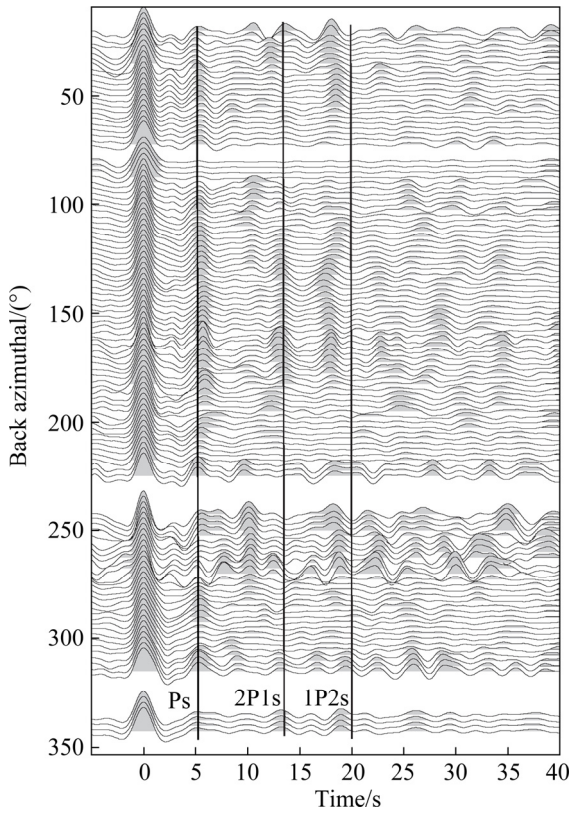

Fig. 3 SV receiver functions at station ZJ.CHA

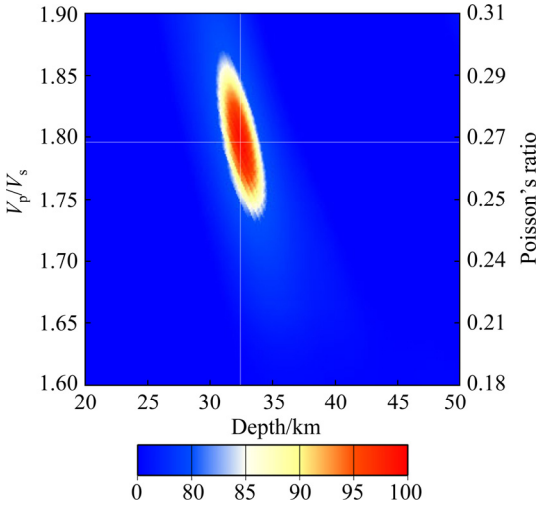

Fig. 4 *H*–*κ* stacking results at station ZJ.CHA (Center of ellipsis representing the best estimates of *H* and *κ*)

Moreover, we also calculated the measured error ignoring the high-order terms using the root mean square error of Moho depth (δ_H) and V_p/V_s ratio (δ_κ) based on the Taylor expansion. The measured error equations can be written as Eq. (3) [30]:

$$\begin{cases}\delta_H^2=2\delta_s/\dfrac{\partial^2 S}{\partial H^2}\\ \delta_\kappa^2=2\delta_s/\dfrac{\partial^2 S}{\partial \kappa^2}\end{cases} \quad (3)$$

where δ_s indicates the variance of the objective function $S(H, \kappa)$.

4.2 Poisson's ratio

We obtained Moho depth (*H*) and average crustal V_p/V_s ratio (*κ*) using the receiver function technique. Since Poisson's ratio is relatively sensitive to the composition of the crustal rock [31], it was then determined by V_p/V_s ratio using Eq. (4):

$$\sigma=0.5-\frac{1}{2[(V_p/V_s)^2-1]} \quad (4)$$

Crustal thickness was further computed from the seal level by subtracting station elevations from the measured *H*. Both crustal thickness and Poisson's ratio were also used to discuss crustal composition.

5 Results

5.1 Moho depth

We obtained 207 robust measurements of

Moho depth and 207 values of V_p/V_s and 207 values of Poisson's ratio. The measured Moho depth and Poisson's ratio are further interpolated into meshed 0.25°×0.25° grids of the study area (Fig. 5). The Moho depth beneath the YB varies from 31.5 to 54.9 km, with an average of 40.1 km, which is significantly higher than that in the CB. Note that the average crustal thickness beneath Sichuan Basin is large and reaches ~42 km, which is consistent with the former studies [24,32]. The Moho depth beneath the CB is in the range of 24.0−35.4 km with an average of ~28.7 km. The Moho depth in the northeastern CB is slightly deeper than that in the southeastern CB, which may be related to the distinct tectonic terranes (Wuyishan terrane and Nanling—Yunkai terrane) [33]. Compared with the flat and shallow Moho surface (27−28 km) in the southwestern CB, Moho depth in the northeastern CB is relatively deep, with an average depth of 31 km. Moho depth is gradually reduced from the west to the western boundary. A large offset of crustal thickness is approximately 5 km on both sides of the buried Jiujiang—Shitai Fault, indicating that this fault is a major tectonic boundary between the YB and CB.

In the eastern region of our study area, we observed an average Moho depth of ~31 km (Fig. 5(a)). Moho relief is approximately 30 km in the CB and ~32 km in the Lower Yangtze Block (LYB) (Fig. 5(a)). An average crustal thickness of

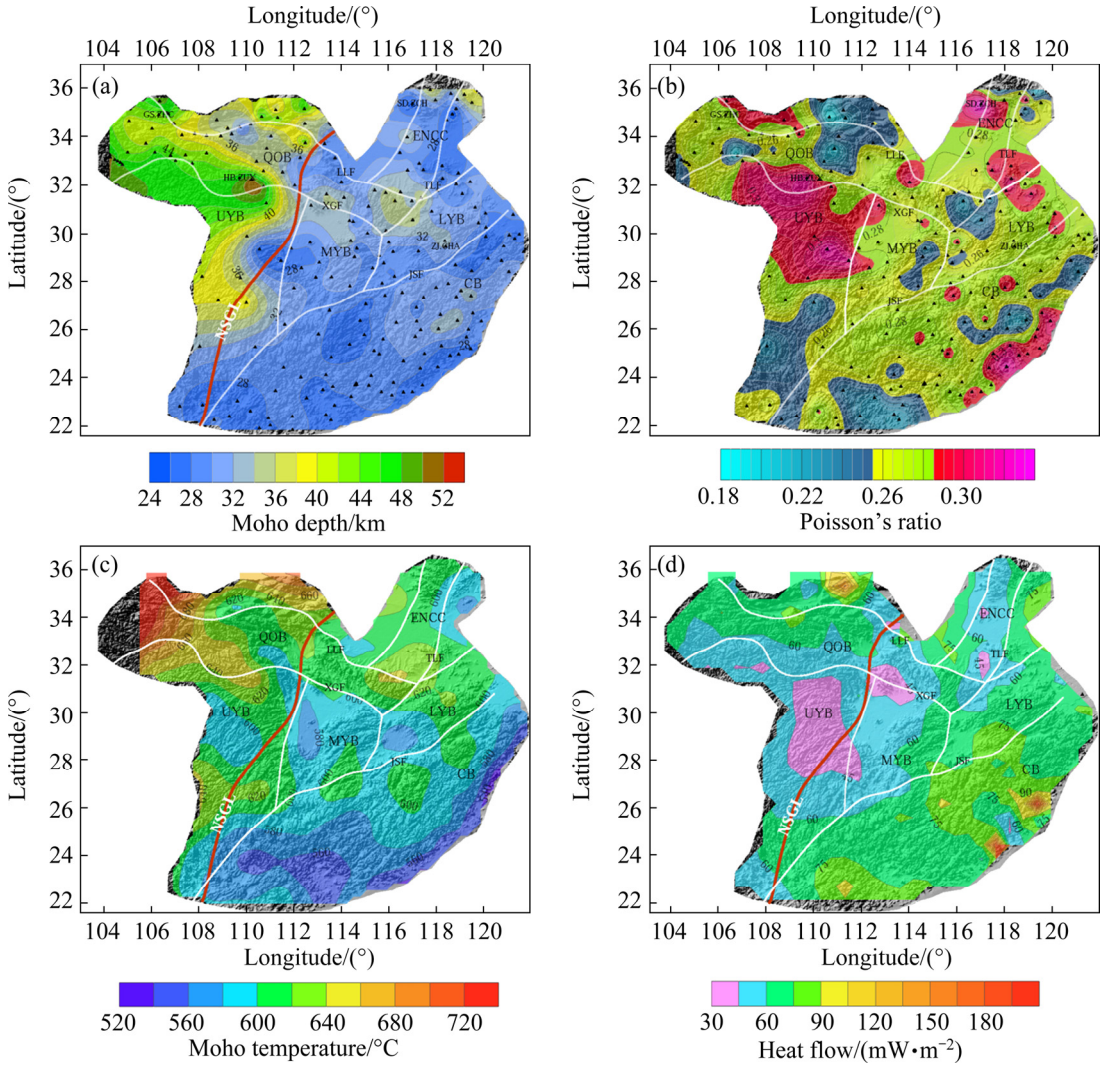

Fig. 5 Estimated relief maps of Moho depth and Poisson's ratio: (a) Lateral variation in Moho relief; (b) Lateral distribution of Poisson's ratio; (c) Moho temperature [34,35]; (d) Surface heat flow [36] (Block triangles in (a, b) represent seismic stations. White solid lines represent tectonic units and major faults (ENCC: Eastern North China Craton; CB: Cathysia Block; YB: Yantaze Block; DB: Dabie Block; QOB: Qinling Orogenic Belt; TNL: Tanlu Fault; LLF: Luonan—Luanchuan Fault; XGF: Xiangfan—Guangji Fault; JSF: Jiangshan—Shaoxing Fault))

~33 km is observed in the Middle Yangtze Block (MYB), while a relatively deeper Moho depth of 43 km is observed in the western portion of North−South trending Gravity Lineament (NSGL) and 46 km is observed in the Upper Yangtze Block (UYB) (Fig. 5(a)). Moho relief is deeper in the western Qinling Orogenic Belt (QOB). The measured Moho depth beneath two seismic stations (HB.ZUX and GS.ZHC) located in the South Qinling Block (SQB) showed significantly deep values of 56.6 and 42.9 km (Fig. 5(a)). The measured crustal thickness extends to ~40 km beneath the NCC and Weihe Basin.

5.2 Poisson's ratio

The measured Poisson's ratio is an elastic property for the crustal rock which is determined from Eq. (4). We found that most of Poisson's ratios were larger than 0.26 in the eastern NCC, with the highest value, 0.333, at SD.ZCH and SD.JUX stations (Fig. 5(b)). The average measured Poisson's ratio in the QOB and Dabie terrane was ~0.257, while the relatively high Poisson's ratio was approximately 0.286 in the UYB and the southwestern portion of NSGL. In the MYB and central to the eastern CB, Poisson's ratio varied from 0.257 to 0.286. The measured high value of Poisson's ratio (>0.295) was obvious in the southern CB (Fig. 5(b)).

6 Discussion

6.1 Crustal structure and magmatic event

We observed shallow Moho depth in eastern China, extending deeply towards the western section of the study area. Our observed thick crust and high Poisson's ratio in the western study are consistent with those reported in previous studies [24,32,33]. The estimated Moho depth was shallow (~31 km) beneath the Tanlu shear zone and SE China (Fig. 5(a)). Late Mesozoic asthenosphere upwelling was widely recognized in the southern Tanlu area and SE China, and caused lithospheric extension and thinning [29]. The thin crustal thickness in the eastern portion of NSGL could be considered as a consequence of the delamination process associated with collision of the NCB and SCB [37−39]. Our measured crustal thickness in the QOB varied from 36 to 38 km and reached ~42 km in the Trans North China Orogen (TNCO) (Fig. 5(a)). The measured crustal thickness was ~32 km in the Lower Yangtze Block (LYB), ~33 km in the MYB, and 46 km in the UYB, which are consistent with previous studies [40,41]. Petrochemical analysis of rock samples in the QOB established a relationship between crustal thickness and geochemistry in magmatic arcs [42−45]. Geological data suggested a 1300 km wide intracontinental orogen and postorogenic magmatic province in Mesozoic South China [4]. We then deduced that this thin crust in the SE China might link to the rollback of subducted Paleo-Pacific slab, which triggered the delamination phenomenon [14,37−39] and thermochemical erosion in the region [42].

6.2 Poisson's ratio and minerals deposits

CHRISTENSEN [31] argued that Poisson's ratio is relatively sensitive to the composition of the crustal rocks and the percentage content of silica. In general, the silica content in the crust affected the value of Poisson's ratio. On the other hand, mafic-ultramafic or partial melt could also increase the value of Poisson's ratio [46]. Poisson's ratio varied with different mineral contents, such as felsic contents (<0.260), intermediate contents (0.260−0.280), and mafic contents (>0.280). We then deduced that the low Poisson's ratio (<0.260) in the QOB might be related to the high felsic content in the crust, whereas the intermediate Poisson's ratio could reflect the intermediate-mafic content in the lower crust. GAO et al [44] analyzed 4500 rock samples in the QOB and revealed that the lower crust was predominately composed of granodioritic to quartz-dioritic rocks. Hence, the relatively high values of Poisson's ratio around the Tanlu Fault, along with the eastern NCC and Sulu Orogen might attribute to mafic anomalies in the lower crust (Fig. 6). The Adakites (high-Sr granitoids) are typically distinct rocks that contain diamonds or coesites in the east of Tanlu Fault (Fig. 6) [2,47]. Geological data showed that these types of rocks are generally formed by partial melting of the thick lower crust during delamination in the subduction zone [13,46]. The measured lower Poisson's ratio (~0.265) around the MYB, LYB and the central CB might suggest felsic lower crust beneath these areas. In the Dehua gold ore field, the observed high Poisson's ratio (0.295) could be caused by mafic underplating, which was explained by geophysical

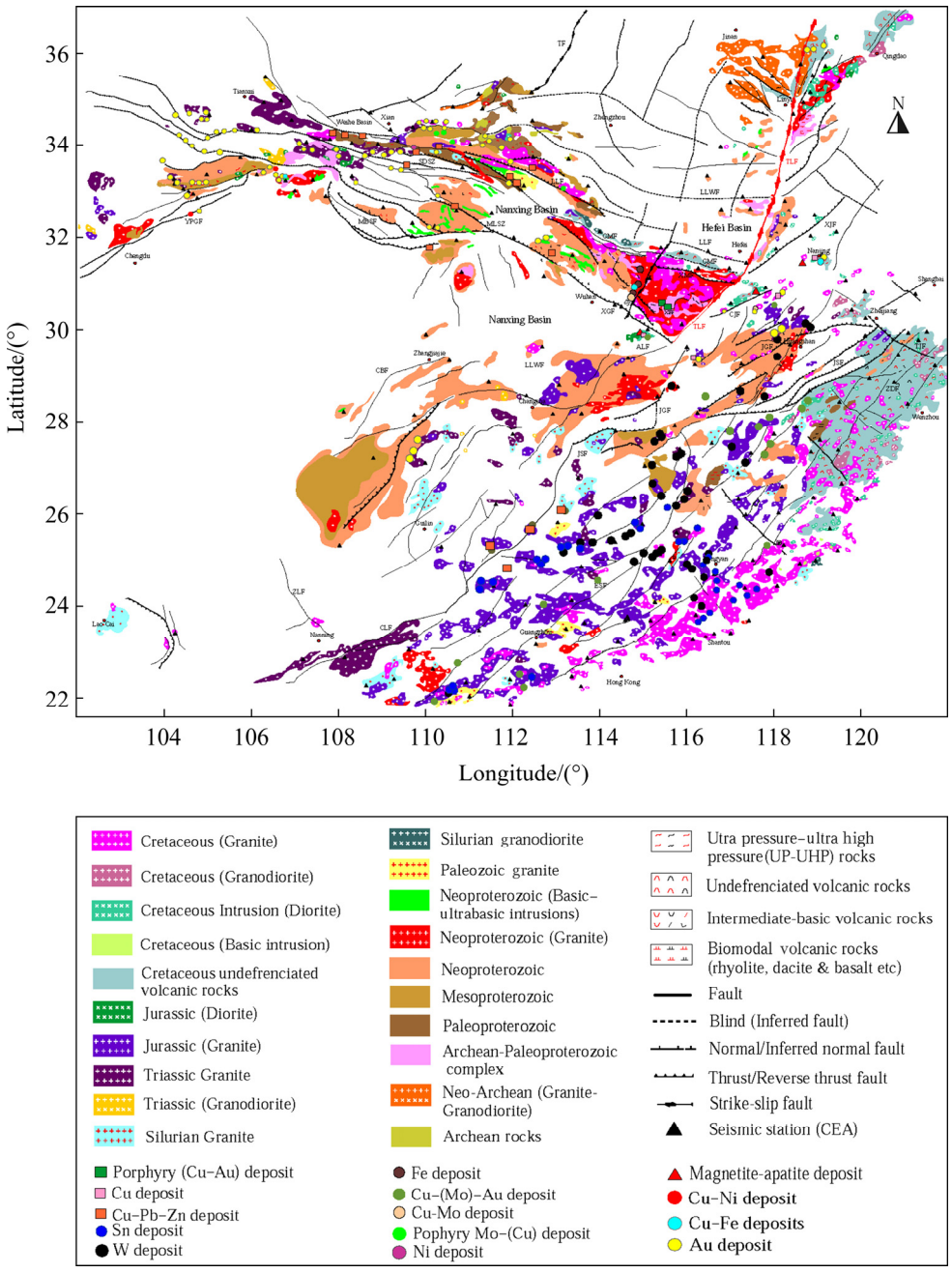

Fig. 6 Geological and metallic minerals deposits map in SE China (JOB: Jiangnan Orogenic Belt; ENCC: Eastern North China Craton; TNCO: Trans-North China Orogen; CB: Cathysia Block; YB: Yantaze Block; DB: Dabie Complex; SQB: South Qinling Block; NQB: North Qinling Block; SO: Sulu Orogen; TF: Taihang Fault; TNL: Tanlu Fault; LLF: Luonan—Luanchuan Fault; ESF: Enping—Shaoxing Fault; LLWF: Lingbo—Lushan—Wuyang Fault; GMF: Guishan—Meishan Fault; ZLF: Ziyun—Luoding Fault; XMF: Xiaotaian—Mozitan Fault; JXF: Jiashan—Xiangshui Fault; ALF: Anhua—Luocheng Fault; XTF: Xishui—Tongcheng Fault; MLSZ: Mainlue-Suture-Zone; SMF: Shangcheng—Machang Fault; QYSF: Qiyueshan Fault; YPGF: Yangpingguan Fault; CLF: Chenzhou—Linwu Fault; DWF: Dawu Fault; XGF: Xiangfan—Guangji Fault; MBSF: Mainlue—Bashan—Xiangguan Fault; CBF: Cili—Baojing Fault; CJF: Changjiang Fault; JSF: Jiangshan—Shaoxing Fault; TJF: Turong—Jianyang Fault; JGF: Jiangnan Fault; QPF: Qiping Fault; ZDF: Zhenghe—Dapu Fault) (modified from Refs. [2,47])

studies [3,4,39−41]. All these measured results suggested that a Mesozoic mantle-derived mafic magma stored in the middle-lower crust mixed with felsic crust, and those also indicated that the mixed magma generally acted as a sources of Mesozoic felsic magmatism in SE China (Fig. 6).

Moreover, our measured results showed a high Poisson's ratio (0.283−0.313) in the northwestern UYB, which indicated mafic minerals in the crust and granodiorite-ultrabasic intrusion in the Meso-Neoproterozoic basement (Fig. 6). There were two prominent high seismic velocity anomalies beneath two domes (Haungling—Shennogjia Massifs and Shennongjia—Huangling) on the northern edge of the UYB [48−50]. Our measured Poisson's ratio (0.313) was also relatively high around these two domes. Geological data showed that a consistency in location with a rapidly uplifted area beneath these areas since 15 Ma [48], implying the asthenospheric flux from the Tibetan Plateau [49,50]. Due to the high percent of gabbro and peridotite or dunite in mafic/ultramafic igneous rocks, the high Poisson's ratio for these igneous rocks might be related to either a high percentage of Mg to Fe or predominantly dunite to anorthosite in the lower crust (Figs. 5(b) and 6), which is consistent with recent studies [51,52]. On the other hand, the high Poisson's ratio (0.318) in the southeastern margin of the CB might have been caused by Yanshanian magmatism in the Cretaceous. In addition, partial melting could also have significantly reduced the velocity of the shear wave and increased the Poisson's ratio [13,46].

6.3 Thermal crustal structure and Poisson's ratio

OHNO et al [34] employed an empirical formula on P wave velocity to calculate the thermal structure in China and determined that the Moho temperature beneath the Precambrian Cratons (NCC and SCB) ranged from 520 to 720 °C (Fig. 5(c)). WEI and SHEN [36] evaluated the heat flow in mainland China (Fig. 5(d)) and found that Moho temperature had a sharp variation across the QOB, Sulu Orogen (SO), and ENCC (Fig. 5(c)). The orogenic belts, high heat flow and high temperature might represent shear heating as a result of active collisional zones.

CHRISTENSEN [31] studied the velocity of compressional wave and shear wave with several common rock samples at different temperatures and pressures and pointed out that quartz-bearing granite and granulite decreased Poisson's ratio with increasing temperature up to 500 °C [34,35]. However, JI et al [26,27] reported the measurements of V_p and V_s of polycrystalline quartzite at a pressure of 600 MPa and suggested that Poisson's ratio decreases smoothly with increasing temperature to ~450 °C. In contrast, Poisson's ratio decreased abruptly at the $\alpha-\beta$ quartz transition at a temperature of ~650 °C. However, Poisson's ratio increased suddenly with rising temperature between 650 and 710 °C after the transition of β quartz. Nevertheless, JI et al [27] studied the quartz-bearing rocks, such as granite, diorite, and felsic gneiss, and showed the $\alpha-\beta$ quartz transition only across the middle-lower crustal boundary. The value of V_p/V_s ratio and Poisson's ratio were low in quartz-rich continental crust with a high geothermal anomaly (dT/dz> 25 °C/km) [41,42]. We followed previous studies and drew Moho temperature in our study area. Moho temperature in the eastern region of NSGL is less than ~640 °C, while the temperature gradually increases up to ~700 °C in the WQOB (Fig. 5(c)) [35]. Due to the lower mafic crustal flow, Moho temperature in the WQOB was relatively high [34,35]. We deduced that the high Poisson's ratio in certain locations in thin crustal regions might be attributed to the underplating of partial mafic melt and high mafic granulite and anorthosite.

6.4 Relationship between metallic ore deposits and crustal composition

The MLYMB was considered to be an important mineral resource in China, and was enriched in polymetallic deposits (Au, Ag, Cu, Fe, Zn, Pb and Mo) [51−53]. Ore clusters including Ningwu (Fe), Anqing—Guichi (Cu, Fe), Luzong (Fe, Cu), Tongling (Cu, Au, Pb, Zn), Edong (Fe, Cu), Ningzhen (Cu, Fe, Pb, Zn) and Jiurui (Cu, Au) spread in the MLYMB area from the northeast to southwest (Fig. 6) [52]. In the Ningzhen and Ningwu clusters, we observed a high Poisson's ratio (>0.284) (Figs. 5(b) and 6). Since these clusters generally host Cretaceous rocks (granitic−volcanic and dioritic) with enormous metalogic deposits (Au, Cu, Mo and Fe) [10,51], we infer that the measured high Poisson's ratio could be attributed to the lower mafic crustal composition in the MLYMB.

Mineral systems were the products of metallogenic processes associated with the

geodynamic evolution of tectonic plates and their ultimate amalgamation. Combined the above research results and geological data, we conclude that the Mesozoic (Yanshanian) magmatic event might have caused stretching, extension, and deformation of the crustal structure that originated from the metallogeny in the region. In addition, this mineralization might be related to plutonic (intrusive, granitic−dioritic) and volcanic igneous rocks. In this study, we further developed a correlation between Poisson's ratio and the orogenic and hydrothermal deposits associated with the Yanshanian magmatic event. The mechanisms for the mineral of these ore deposits are linked to the region's tectonic evolution and magmatic event [54−56]. We also pointed out that several magmatic activities have distributed in the metallogenic system across SE China since the Phanerozoic (Fig. 6).

7 Conclusions

(1) The measured results showed both high Poisson's ratio and the average thick crust (~43 km) spread in the western portion of NSGL, and a relatively low Poisson's ratio and thin crust (~27 km) in the eastern portion of NSGL.

(2) Compared Poisson's ratio to metallogenic mineralization and magmatic event, we found that Poisson's ratio could reflect different crustal compositions, which include felsic (<0.260), intermediate (0.260−0.280), and mafic (>0.280). Combined with the geological data, we pointed out that the high Poisson's ratio in the middle and upper of the Yangtze Craton might be related to the high Fe or Mg content in the middle-lower crust. Moreover, mafic granulite and anorthosite materials in the middle to lower crust can also increase Poisson's ratio up to ~0.286 and ~0.313, respectively.

(3) The high Poisson's ratio for crustal rock in the southeastern margin of the CB might be related to Mesozoic mafic partial melt, which provides an important environment for various magmatic intrusions and metallogenies. This mafic melt mixed with crustal felsic materials in the lower crust might result in magmatism and mineralization in the region.

(4) Compared Poisson's ratio of the intrusive deposits to that of igneous volcanic complexes, we deduced that the metallic mineral system might be associated with orogenic and hydrothermal deposits. These results indicated that multistage magma and mineralization in our study area might be attributed to the tectonic-magma-thermal event.

Acknowledgments

We thank the Data Management Center of China Earthquake Administration for providing the waveform data for this study. This study is financially supported by the National Natural Science Foundation of China (Nos. 41974049, 42074165), and the Science and Technology on Parallel and Distributed Processing Laboratory, China (No. 6142110180202).

References

[1] TENG Ji-wen. Prospecting for metal ore deposits in second deep space of crustal interior, the building of strategy reserve base of northeast China [J]. Journal of Jilin University (Earth Science Edition), 2007, 37(4): 633−651. (in Chinese)

[2] PIRAJNO F. The geology and tectonic settings of China's mineral deposits [M]. Dordrecht, Netherlands: Springer Science & Business Media, 2012.

[3] ZHOU Xin-min, LI Wu-xian. Origin of Late Mesozoic igneous rocks in Southeastern China: Implications for lithosphere subduction and underplating of mafic magmas [J]. Tectonophysics, 2000, 326: 269−287.

[4] LI Zheng-xiang, LI Xian-hua. Formation of the 1300 km-wide intracontinental orogen and postorogenic magmatic province in Mesozoic South China: A flat-slab subduction model [J]. Geology, 2007, 35: 179−182.

[5] YANG Xiao-yong, SUN Wei-dong. Jurassic and Cretaceous (Yanshannian) tectonics, magmatism and metallogenesis in South China: Preface [M]. Oxfordshire: Taylor & Francis, 2018.

[6] WINDLEY B, MARUYAMA S, XIAO Wen-jiao. Delamination/thinning of sub-continental lithospheric mantle under Eastern China: The role of water and multiple subduction [J]. American Journal of Science, 2010, 310(10): 1250−1293.

[7] MAO Jing-wen, PIRAJNO F, COOK N. Mesozoic metallogeny in East China and corresponding geodynamic settings — An introduction to the special issue [J]. Ore Geology Reviews, 2011, 43: 1−7.

[8] MAO Jing-wen, XIE Gui-qing, DUAN Chao, PIRAJNO F, ISHIYAMA D, CHEN Yu-chuan. A tectono-genetic model for porphyry–skarn–stratabound Cu−Au−Mo−Fe and magnetite–apatite deposits along the Middle-Lower Yangtze

River Valley, Eastern China [J]. Ore Geology Reviews, 2011, 43(1): 294−314.

[9] SHU Liang-shu, ZHOU Xin-min, DENG Peng, WANG Bo, JIANG Shao-yong, YU Jin-hai, ZHAO Xi-xi. Mesozoic tectonic evolution of the Southeast China Block: New insights from basin analysis [J]. Journal of Asian Earth Sciences, 2009, 34(3): 376−391.

[10] CHEN Guang-hao, LIANG Guang-he, XU De-ru, ZENG Qiao-song, FU Shou-hui, WEI Xiang-rong, HE Zhuan-li, FU Gong-gu. Application of a shallow seismic reflection method to the exploration of a gold deposit [J]. Journal of Geophysical Engineering, 2004, 1: 12−16.

[11] LIU Guo-feng, MENG Xiao-hong, NI Jian-hui, CHEN Zhao-xi, ZHANG Da. Evaluation of the 2D reflection seismic method toward the exploration of thrust-controlled mineral deposits in southwestern Fujian Province, China [J]. Geophysics, 2018, 83: B209−B220.

[12] LUO Song, YAO Hua-jian, LI Qiu-sheng, WANG Wei-tao, WAN Ke-song, MENG Ya-feng, LIU Bin. High-resolution 3D crustal S-wave velocity structure of the Middle-Lower Yangtze River Metallogenic Belt and implications for its deep geodynamic setting [J]. Science China Earth Sciences 2019, 62: 1361−1378. (in Chinese)

[13] XU Ji-feng, SHINJO R, DEFANT M, WANG Qiang, RAPP R. Origin of Mesozoic adakitic intrusive rocks in the Ningzhen area of east China: Partial melting of delaminated lower continental crust? [J]. Geology, 2002, (30)12: 1111−1114.

[14] LIU Lei, XU Xi-sheng, XIA Yan. Asynchronizing paleo-pacific slab rollback beneath SE China: Insights from the episodic Late Mesozoic volcanism [J]. Gondwana Research, 2015, 37: 397−407.

[15] SUN Wei-dong, LING Ming-xing, YANG Xiao-yong, FAN Wei-ming, DING Xing, LIANG Hua-ying. Ridge subduction and porphyry copper-gold mineralization: An overview [J]. Science in China, Series D: Earth Sciences, 2010, 53: 475−484. (in Chinese)

[16] ZHAI Ming-guo, SANTOSH M. The early Precambrian odyssey of the North China Craton: A synoptic overview [J]. Gondwana Research, 2011, 20: 6−25.

[17] HUANG Ti-qing, REN Ji-shun, JIANG Chuan-fa, ZHANG Zhi-meng, XU Zhi-qin. An outline of the tectonic characteristics of China [J]. Acta Geological Sinica, 1977, 36: 288−303. (in Chinese)

[18] YIN An. Cenozoic tectonic evolution of Asia: A preliminary synthesis [J]. Tectonophysics, 2010, 488: 293−325.

[19] WANG Yue-jun, FAN Wei-ming, ZHANG Guo-wei, ZHANG Yan-hua. Phanerozoic tectonics of the South China Block: Key observations and controversies [J]. Gondwana Research, 2013, 23: 1273−1305.

[20] HOU Zeng-qian, YANG Zhu-sen, SHI Da-nian. Underplating in the middle-lower Yangtze Valley and model of geodynamic evolution: Constraints from geophysical data [J]. Science in China, Series D: Earth Sciences, 2005, 48(7): 985−999. (in Chinese)

[21] ZHENG Jian-ping, GRIFFIN W, O'REILLY S, ZHANG Ming, PEARON N, PAN Yuan-ming. Widespread Archean basement beneath the Yangtze craton [J]. Geology, 2006, 34: 417−417.

[22] DONG Shu-wen, GAO Rui, YIN An, GUO Tong-lou, ZHANG Yue-qiao, HU Jian-min, LI Jian-hua, SHI Wei, LI Qiu-sheng. What drove continued continent−continent convergence after ocean closure? Insights from high-resolution seismic-reflection profiling across the Daba Shan in central China [J]. Geology, 2013, 41(6): 671−674.

[23] ZANDT G, AMMON C. Continental crust composition constrained by measurements of crustal Poisson's ratio [J]. Nature, 1995, 374: 152−154.

[24] SUN Ya, NIU Feng-lin, LIU Hua-feng, CHEN You-lin, LIU Jian-xin. Crustal structure and deformation of the SE Tibetan plateau revealed by receiver function data [J]. Earth and Planetary Science Letters, 2012, 349: 186−197.

[25] NIU Feng-lin, LI Juan. Component azimuths of the CEArray stations estimated from P-wave particle motion [J]. Earthquake Science, 2011, 24: 3−13. (in Chinese)

[26] JI Shao-cheng, LI Le, MOTRA H, WUTTKE F, SUN Sheng-si, MICHIBAYASHI K, SALISBURY M. Poisson's ratio and auxetic properties of natural rocks [J]. Journal of Geophysical Research: Solid Earth, 2018, 123(2): 1161−1185.

[27] JI Shao-cheng, SUN Sheng-si, WANG Qian, MARCOTTE D. Lamé parameters of common rocks in the Earth's crust and upper mantle [J]. Journal of Geophysical Research: Solid Earth, 2010, 115(B6): 1−15.

[28] SUN Ya, LIU Jian-xin, ZHOU Ke-ping, CHEN Bo, GUO Rong-wen. Crustal structure and deformation under the Longmenshan and its surroundings revealed by receiver function data [J]. Physics of the Earth and Planetary Interiors, 2015, 244: 11−22.

[29] CHEN Ling, ZHENG Tian-yu, XU Wei-wei. A thinned lithospheric image of the Tanlu Fault Zone, eastern China: Constructed from wave equation-based receiver function migration [J]. Journal of Geophysical Research: Solid Earth, 2006, 111(B9): 1−15.

[30] ZHU Lu-pei, KANAMORI H. Moho depth variation in Southern California from teleseismic receiver functions [J]. Journal of Geophysical Research, 2000, 105, 2969−2980.

[31] CHRISTENSEN N. Poisson's ratio and crustal seismology [J]. Journal of Geophysical Research: Solid Earth, 1996, 101(B2): 3139−3156.

[32] ZHANG Pan, ZHU Liang-bao, CHEN Hao-peng, WANG Qing-dao, YANG Ying-hang. Crustal structure in China from teleseismic receiver function [J]. Acta Seismological Sinica, 2014, 36(5): 850−861. (in Chinese)

[33] LÜ Qing-tian, SHI Da-nian, LIU Zhen-dong, ZHANG Yong-qian, DONG Shu-wen, ZHAO Jin-hua. Crustal structure and geodynamics of the Middle and Lower reaches of Yangtze metallogenic belt and neighboring areas: Insights from deep seismic reflection profiling [J]. Journal of Asian Earth Sciences, 2015, 114: 704−716.

[34] OHNO I, HARADA K, YOSHITOMI C. Temperature variation of elastic constants of quartz across the α–β transition [J]. Physics and Chemistry of Minerals, 2006, 33(1): 1−9.

[35] LAKSHTANOV D, SINOGEIKIN S, BASS J. High-temperature phase transitions and elasticity of silica polymorphs [J]. Physics and Chemistry of Minerals, 2007, 34(1): 11−22.

[36] WEI Tao, SHEN Zheng-kang. Heat flow distribution in Chinese continent and its adjacent areas [J]. Progress in Natural Science, 2008, 18(7): 843−849.

[37] DENG Yang-fan, LEVANDOWSKI W. Lithospheric alteration, intraplate crustal deformation, and topography in eastern China [J]. Tectonics, 2018, 37: 4120−4134.

[38] GUO Run-hua, LI Shan-zhong, SUO Yan-hui, WANG Qian, ZHAO Shu-juan, WANG Yi-qi, GUO Ling-li. Indentation of North China Block into Greater South China Block and Indosinian Orocline [J]. Earth Science Frontiers, 2017, 24: 171−184. (in Chinese)

[39] LI Xiao-yong, ZHU Pei-min, KUSKY T, GU Yuan, PENG Song-bai, YUAN Yue-feng, FU Jian-min. Has the Yangtze craton lost its root? A comparison between the North China and Yangtze Cratons [J]. Tectonophysics, 2015, 655: 1−14.

[40] HE Chuan-song, DONG Shu-wen, SANTOSH M, CHEN Xuan-hua. Seismic evidence for a geosuture between the Yangtze and Cathaysia Blocks, South China [J]. Scientific Reports, 2013, 3(2200): 1−7.

[41] HUANG Rong, XU Yi-xian, ZHU Lu-pei, HE Kai. Detailed Moho geometry beneath southeastern China and its implications on thinning of continental crust [J]. Journal of Asian Earth Sciences, 2015, 112: 42−48.

[42] SUN Yu-jun, DONG Shu-wen, ZHANG Huai, LI Han, SHI Yao-lin. 3D thermal structure of the continental lithosphere beneath China and adjacent regions [J]. Journal of Asian Earth Sciences, 2013, 62: 697−704.

[43] WU Yuan-bao, ZHENG Yong-fei. Tectonic evolution of a composite collision orogen: An overview on the Qinling—Tongbai—Hong'an—Dabie—Sulu Orogenic Belt in central China [J]. Gondwana Research, 2013, 23: 1402−1428.

[44] GAO Shan, ZHANG Ben-ren, LUO Yan, LI Xian-hua. Chemical composition of the continental crust in the Qinling Orogenic Belt and its adjacent North China and Yangtze Cratons [J]. Geochimica et Cosmochimica Acta, 1992, 56(11): 3933−3950.

[45] WANG Min. Study on present-day crustal deformation in China [J]. Recent Developments in World Seismology, 2010(3): 39−41.

[46] HE Yong-sheng, LI Shu-guang HOEFS J, HUANG Fang, LIU Sheng-ao, HOU Zhen-hui. Post-collisional granitoids from the Dabie orogen: New evidence for partial melting of a thickened continental crust [J]. Geochimica et Cosmochimica Acta, 2011, 75(13): 3815−3838.

[47] WANG Qiang, DEREK A, XU Ji-feng, ZHAO Zhen-hua, JIAN Ping, XIONG Xiao-lin, BAO Zhi-wei, LI Chao-feng, BAI Zheng-hua. Petrogenesis of Cretaceous adakitic and shoshonitic igneous rocks in the Luzong area, Anhui Province (eastern China): Implications for geodynamics and Cu−Au mineralization [J]. Lithos, 2006, 89: 424−446.

[48] HU Fang-yang, DU Mi-hai, LIU Shu-wen, CHAPMAN J. Quantifying crustal thickness in continental collisional belts: Global perspective and a geologic application [J]. Scientific Reports, 2017, 7: 7058−7058.

[49] ZHAI Ming-guo, FAN Qi-cheng, ZHANG Hong-fu, SUI Jian-li. Lower crustal processes leading to Mesozoic lithospheric thinning beneath eastern North China: Underplating, replacement and delamination [J]. Lithos, 2007, 96: 36−54.

[50] SUN Ya, LIU Jian-xin, TANG You-cai, CHEN Jia-wei, ZHOU Ke-ping, CHEN Bo. Structure of the upper mantle and transition zone beneath the South China Block imaged by finite frequency tomography [J]. Acta Geologica Sinica: English Edition, 2016, 90(5): 1637−1652.

[51] PAN Yuan-ming, DONG Ping. The Lower Changjiang (Yangzi/Yangtze River) metallogenic belt, east central China: Intrusion and wall rock-hosted Cu−Fe−Au, Mo, Zn, Pb, Ag deposits [J]. Ore Geology Reviews, 1999, 15: 177−242.

[52] GU Huang-ling, YANG Xiao-yong, NIE Zhang-xing, DENG Jiang-hong, DUAN Liu-an, HU Qing. Study of Late-Mesozoic magmatic rocks and their related copper-gold-polymetallic deposits in the Guichi ore-cluster district, Lower Yangtze River Metallogenic Belt, East China [J]. International Geology Review, 2018, 60: 1404−1434.

[53] PENG Ying-hao, LIU Chong-yu, WEI Li-li, JIANG Hong-jie, GE Zhen-jiang. Quench sensitivity and microstructures of high-Zn-content Al−Zn−Mg−Cu alloys with different Cu contents and Sc addition [J]. Transactions of Nonferrous Metals Society of China, 2021, 31(1): 24−35.

[54] ZHANG Qi. The characteristics and tectono-metallogenic significance of the adakites in Yanshan period from eastern China [J]. Acta Petrologica Sinica, 2001, 17: 236−244. (in Chinese)

[55] WEI Zi-gen, CHEN Ling, LI Zhi-wei, LING Yuan, LI Jing. Regional variation in Moho depth and Poisson's ratio beneath eastern china and its tectonic implications [J]. Journal of Asian Earth Sciences, 2016, 115: 308−320.

[56] CHEN Yan-jing, CHEN Hua-yong, ZAW Khin, PIRAJNO F, ZHANG Zeng-Jie. Geodynamic settings and tectonic model of skarn gold deposits in China: An overview [J]. Ore Geology Reviews, 2007, 31: 139−169.

基于接收函数的中国东南部区域深部成矿机制

柳建新[1,2,3], Syed muzyan SHAHZAD[1,2,3], 孙 娅[1,2,3],
Asim SHAHZAD[1], 李 川[4], Meryem FANIDI[1,2], Ishfaque MUHAMMAD[1]

1. 中南大学 地球科学与信息物理学院，长沙 410083；
2. 中南大学 有色金属成矿预测与地质环境监测教育部重点实验室，长沙 410083；
3. 中南大学 有色资源与地质灾害探查湖南省重点实验室，长沙 410083；
4. 桂林理工大学 地球科学学院，桂林 541006

摘 要：中国东南部地区的地壳变形机制和深部成矿机制一直存在争议。本研究基于中国地震台网 207 个地震站观测到的地震波形数据，采用接收函数方法计算中国东南部的地壳厚度和地壳内岩石的泊松比。结果表明，研究区东部地壳厚度约为 27 km，而西部地壳厚度约为 43 km，平均地壳厚度为 31 km，地壳呈现西厚东薄趋势。地壳内岩石泊松比的结果显示：华夏块体的南部泊松比较高，平均为 0.295，而秦岭大别造山带的地壳岩石泊松比相对较低，平均为 0.257。在扬子克拉通的中部以及华夏块体的中东部区域，地壳岩石泊松比为 0.257~0.286。通过对比侵入体沉积岩和火成岩的泊松比，初步推断金属矿物系统的形成可能与造山和热液沉积矿床有关，这表明研究区内多期岩浆作用和成矿作用是由构造−岩浆−热事件引起的。而华夏块体东南边缘和上场子克拉通的东北区域地壳岩石的高泊松比可能与中生代中下地壳镁铁质部分熔融有关，同时部分熔融也为岩浆入侵和金属矿床的形成提供了重要环境。

关键词：深部成矿机制；泊松比；中国东南部；地壳厚度

(Edited by Wei-ping CHEN)